Available online at www.sciencedirect.com
ScienceDirect
Journal of Sound and Vibration 315 (2008) 797–815
JOURNAL OF SOUND AND VIBRATION
www.elsevier.com/locate/jsvi

Comparison of robust input shapers

Joshua Vaughan, Aika Yano, William Singhose*

George Woodruff School of Mechanical Engineering, Georgia Institute of Technology, Atlanta, GA 30332–0405, USA

Received 5 April 2007; received in revised form 24 January 2008; accepted 6 February 2008
Handling Editor: P. Davies
Available online 14 April 2008

Abstract

The rapid movement of machines is a challenging control problem because it often results in high levels of vibration. As a result, flexible machines are typically moved relatively slowly. Input shaping is a control method that allows much higher speeds of motion by limiting vibration induced by the reference command. To design an input-shaping controller, estimates of the system natural frequency and damping ratio are required. However, real world systems cannot be modeled exactly, making the robustness to modeling errors an important consideration. Many robust input shapers have been developed, but robust shapers typically have longer durations that slow the system response. This creates a compromise between shaper robustness and rise time. This paper analyzes the compromise between rapidity of motion and shaper robustness for several input-shaping methods. Experimental results from a portable bridge crane verify the theoretical predictions.

1. Introduction

The control of flexible machines is an enormous area of research because all machines will exhibit flexibility when pushed to their performance limits. Much of the work in this area has concentrated on feedback control methods. However, feedback systems can be expensive and difficult to implement, as they require the system to be equipped with sensors. Furthermore, they can require significant computing power and raise the possibility of unstable system behavior. Command shaping methods typically do not have these issues, but they are susceptible to disturbances if they are not used in conjunction with feedback control.

Input shaping reduces vibration by intelligently shaping the reference signal such that the vibratory modes of the system are canceled. To implement this method, the reference signal is convolved with a sequence of impulses, called an input shaper. This process is demonstrated in Fig. 1. The timing and amplitudes of the impulses are determined using estimates of the system frequencies and damping. Note that the rise time of the command is lengthened by the duration of the shaper. In general, the rise time of the input-shaped system will closely track the command rise time, so minimizing the shaper duration is important for achieving high-speed motion.

*Corresponding author. 813 Ferst Dr., Atlanta, GA 30332, USA. Tel.: +1 404 385 0668; fax: +1 404 894 9342.
E-mail address: Singhose@gatech.edu (W. Singhose).

0022-460X/$ - see front matter © 2008 Elsevier Ltd. All rights reserved.
doi:10.1016/j.jsv.2008.02.032

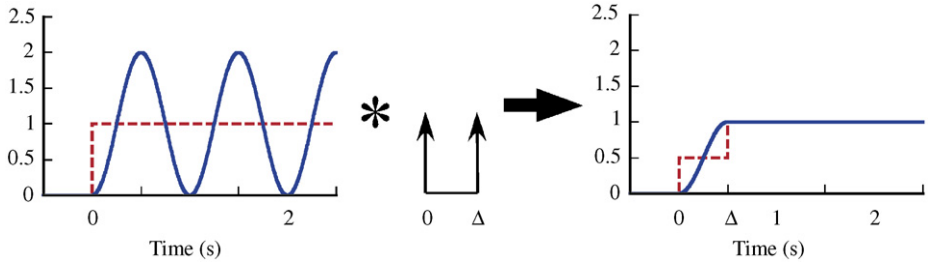

Fig. 1. The input-shaping process, – – command, – response.

While input-shaping methods were first proposed in the 1950s [1–3], the early work was difficult to implement without digital computers. Furthermore, it was sensitive to modeling errors [4]. These early shapers were formed using constraints that limited the residual vibration of the system to zero at the modeled natural frequency and damping ratio. As a result, they are typically referred to as zero vibration (ZV) shapers.

1.1. Input-shaping constraint equations

In order to determine the impulse amplitudes and time locations of an input shaper, the designer must ensure that they satisfy certain design constraints. The primary design constraint is a limit on the amplitude of vibration caused by the shaper. The vibration amplitude of an underdamped, second-order system from a sequence of n impulses is

$$A_{\sum} = \frac{\omega}{\sqrt{1-\zeta^2}} e^{-\zeta\omega t_n} \sqrt{\left(\sum_{i=1}^{n} A_i e^{\zeta\omega t_i} \cos(\omega t_i \sqrt{1-\zeta^2})\right)^2 + \left(\sum_{i=1}^{n} A_i e^{\zeta\omega t_i} \sin(\omega t_i \sqrt{1-\zeta^2})\right)^2}, \tag{1}$$

where ω is the natural frequency of the system, ζ is the damping ratio, and A_i and t_i are the ith impulse amplitude and time, respectively.

To form a nondimensional vibration amplitude, Eq. (1) is divided by the amplitude of residual vibration from a single impulse of unity magnitude. The resulting expression gives the ratio of vibration with input shaping to that without input shaping. The amplitude of residual vibration from a single unity-magnitude impulse applied at time zero is simply

$$A_{\uparrow} = \frac{\omega}{\sqrt{1-\zeta^2}}. \tag{2}$$

Dividing Eq. (1) by Eq. (2) yields the percentage residual vibration (PRV) [5]:

$$\mathrm{PRV} = V(\omega,\zeta) = \frac{A_{\sum}}{A_{\uparrow}} = e^{-\zeta\omega t_n} \sqrt{[C(\omega,\zeta)]^2 + [S(\omega,\zeta)]^2}, \tag{3}$$

where

$$C(\omega,\zeta) = \sum_{i=1}^{n} A_i e^{\zeta\omega t_i} \cos(\omega t_i \sqrt{1-\zeta^2}), \tag{4}$$

$$S(\omega,\zeta) = \sum_{i=1}^{n} A_i e^{\zeta\omega t_i} \sin(\omega t_i \sqrt{1-\zeta^2}). \tag{5}$$

Eq. (3) represents the level of vibration induced by an impulse sequence given any value of frequency and any damping ratio less than one. A constraint on residual vibration amplitude can be formed by setting Eq. (3) less than or equal to a tolerable level of residual vibration at the modeled natural frequency and damping ratio.

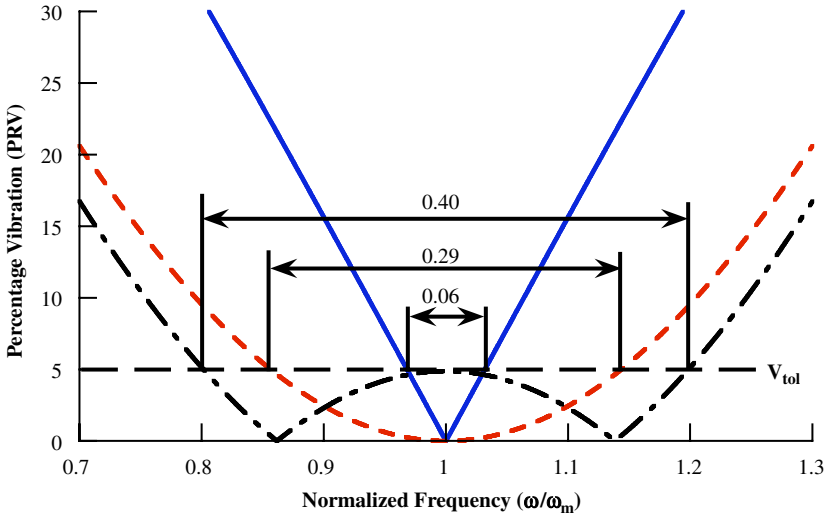

Fig. 2. Sensitivity curves for zero vibration, zero vibration and derivative, and extra insensitive shapers, – zero vibration, – – zero vibration and derivative, – · – extra insensitive.

For the ZV shaper, the tolerable amount of vibration is set to zero. This results in a shaper of the form

$$\mathrm{ZV} = \begin{bmatrix} A_i \\ t_i \end{bmatrix} = \begin{bmatrix} \dfrac{1}{1+K} & \dfrac{K}{1+K} \\ 0 & \dfrac{\tau_d}{2} \end{bmatrix}, \tag{6}$$

where τ_d is the damped vibration period and

$$K = \mathrm{e}^{-\zeta\pi/\sqrt{1-\zeta^2}}. \tag{7}$$

As will be shown in Section 2, additional constraints can be placed on input shapers to ensure robustness to modeling error [6–12].

1.2. Sensitivity curves and insensitivity

Most measures of input-shaping robustness focus on the sensitivity curve of the input shaper. The natural frequency sensitivity curve for a ZV shaper is shown by the solid line in Fig. 2. The vertical axis is the percent residual vibration (PRV) and the horizontal axis is the actual natural frequency, ω, normalized by the modeled frequency, ω_m. The curve indicates how residual vibration changes as a function of modeling errors in frequency. While a sensitivity curve itself is not a measure of robustness, a qualitative picture of the robustness of a command can be obtained from it and quantitative measures can be extracted from it. The various input shapers produce different sensitivity curves because the impulses that comprise the shapers have different amplitudes and time locations.

One key measure of robustness derived from the sensitivity curve is *insensitivity* [12,8]. Insensitivity is the width of the sensitivity curve at a tolerable vibration level, V_{tol}, with respect to the parameter of interest. For example, Fig. 2 shows the ZV shaper has an insensitivity at $V_{\mathrm{tol}} = 5$ percent, $I(5\ \mathrm{percent})$, of 0.06. One drawback with this measure is that it can provide misleading results if applied without common sense. For example, if a sensitivity curve has peaks within the considered range (like the one labeled extra insensitive in Fig. 2), then an automated calculation of insensitivity may be misleading. Consider the case when the peak occurs at 5.1 percent instead of 5 percent. The calculated 5 percent insensitivity width will be zero and falsely indicate that the shaper is not robust. Of course, from a common sense perspective, the robustness is essentially the same if the peak in the sensitivity curve occurs at 5.1 or 5.0 percent.

The large robustness (width of frequency suppression range) provided by both the zero vibration and derivative (ZVD) and extra insensitive (EI) shapers shown in Fig. 2 does not come without cost. Each of these robust shapers (both of which are discussed in Section 2) is longer than the relatively non-robust ZV shaper. This trend continues across all robust shaping methods. In the next section, four robust input-shaping methods will be briefly explained and their sensitivity curves shown. Next, comparisons of robustness and shaper duration are made between methods. Then, experimental results supporting this comparison are presented. The main purpose of these comparisons is to present a clear and concise picture of the compromise between shaper duration and robustness, as well as provide a useful comparison of various robust shapers.

2. Robust shaping details

In real applications, the system parameters needed to form the input shaper are not known exactly. This makes modeling system parameters to within the tolerances needed for ZV shapers difficult. This challenge inspired the development of robust shapers. Numerous robust shapers have been proposed, including input shapers specifically designed to address system nonlinearities such as friction and nonlinear system dynamics [13–16]. The methods used to develop robust shapers fall loosely into four categories: derivative methods, tolerable vibration limit methods, ad hoc methods (e.g. MIS methods discussed in this paper), and numerical optimization methods. For all robust shapers, a compromise must be made between an increase in robustness and the related increase in shaper duration. However, the robustness for a given shaper duration will differ between design methods. Section 3 will evaluate the performance of robust input shapers in terms of this tradeoff.

2.1. Derivative methods

The earliest form of robust input shaping was achieved by setting the derivative, with respect to the frequency, of the residual vibration equation (3) equal to zero [6]:

$$\frac{\partial}{\partial\omega}\left(\mathrm{e}^{-\zeta\omega t_n}\sqrt{[C(\omega,\zeta)]^2+[S(\omega,\zeta)]^2}\right)=0. \tag{8}$$

The resulting shaper is called a zero vibration and derivative (ZVD) shaper. It is described by

$$\mathrm{ZVD}=\begin{bmatrix}A_i\\ t_i\end{bmatrix}=\begin{bmatrix}\dfrac{1}{1+2K+K^2} & \dfrac{2K}{1+2K+K^2} & \dfrac{K^2}{1+2K+K^2}\\ 0 & \dfrac{\tau_d}{2} & \tau_d\end{bmatrix}. \tag{9}$$

Note that the duration of this shaper, $t_3=\tau_d$, is twice that of the ZV shaper, $t_2=\tau_d/2$.

The ZVD shaper sensitivity curve, shown in Fig. 2, has an I(5 percent) of approximately 0.29. The zero derivative constraint flattens the sensitivity curve at the modeled frequency and increases the insensitivity. To further increase insensitivity, this process can be repeated by taking additional, higher-order derivatives, with respect to frequency. The price for each additional derivative, however, is an increase in shaper duration by one-half period of the natural frequency. The next two derivative-method shapers, the zero vibration and double derivative (ZVDD) and zero vibration and triple derivative (ZVDDD), are described by

$$\mathrm{ZVDD}=\begin{bmatrix}A_i\\ t_i\end{bmatrix}=\begin{bmatrix}\dfrac{1}{1+3K+3K^2+K^3} & \dfrac{3K}{1+3K+3K^2+K^3} & \dfrac{3K^2}{1+3K+3K^2+K^3} & \dfrac{K^3}{1+3K+3K^2+K^3}\\ 0 & \dfrac{\tau_d}{2} & \tau_d & \dfrac{3}{2}\tau_d\end{bmatrix} \tag{10}$$

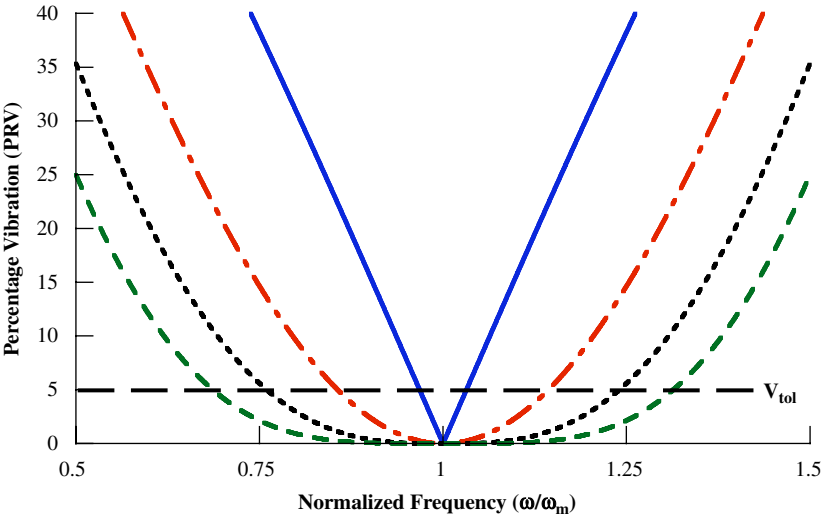

Fig. 3. Sensitivity curves for derivative-method shapers, – zero vibration, – · – zero vibration and derivative, . . . zero vibration and double derivative, – – zero vibration and triple derivative.

and

$$\text{ZVDDD} = \begin{bmatrix} A_i \\ t_i \end{bmatrix} = \begin{bmatrix} \frac{1}{D} & \frac{4K}{D} & \frac{6K^2}{D} & \frac{4K^3}{D} & \frac{K^4}{D} \\ 0 & \frac{\tau_d}{2} & \tau_d & \frac{3}{2}\tau_d & 2\tau_d \end{bmatrix}, \tag{11}$$

where $D = 1 + 4K + 6K^2 + 4K^3 + K^4$. Their sensitivity curves are shown in Fig. 3. The additional insensitivity gained from each higher-order derivative is evident in the plot.

2.2. Tolerable vibration methods

To this point, the shapers discussed have been formed using a constraint that there be zero residual vibration at the modeled frequency. However, even in real world systems for which a good model exists, there will be some modeling error and vibration will occur at the design frequency. Realizing this, the designer should relax this constraint to one in which residual vibration remains below some tolerable level, V_{tol}, at the modeled frequency [8,12]. The first shaper utilizing this idea was called the extra insensitive (EI) shaper. It has a sensitivity curve like the one shown in Fig. 2. The EI shaper has the same impulse times as the ZVD shaper but has different amplitude values that lead to greater robustness. For undamped systems, it has the form [8]

$$\text{EI} = \begin{bmatrix} A_i \\ t_i \end{bmatrix} = \begin{bmatrix} \frac{1+V_{\text{tol}}}{4} & \frac{1-V_{\text{tol}}}{2} & \frac{1+V_{\text{tol}}}{4} \\ 0 & \frac{\tau}{2} & \tau \end{bmatrix}, \tag{12}$$

where V_{tol} is the tolerable level of vibration (e.g. 5 percent $= 0.05$) and τ is the undamped vibration period of the system. For a system with viscous damping, the EI shaper is described by

$$\text{EI} = \begin{bmatrix} A_i \\ t_i \end{bmatrix} = \begin{bmatrix} A_1 & 1-(A_1+A_3) & A_3 \\ 0 & t_2 & \tau_d \end{bmatrix}, \tag{13}$$

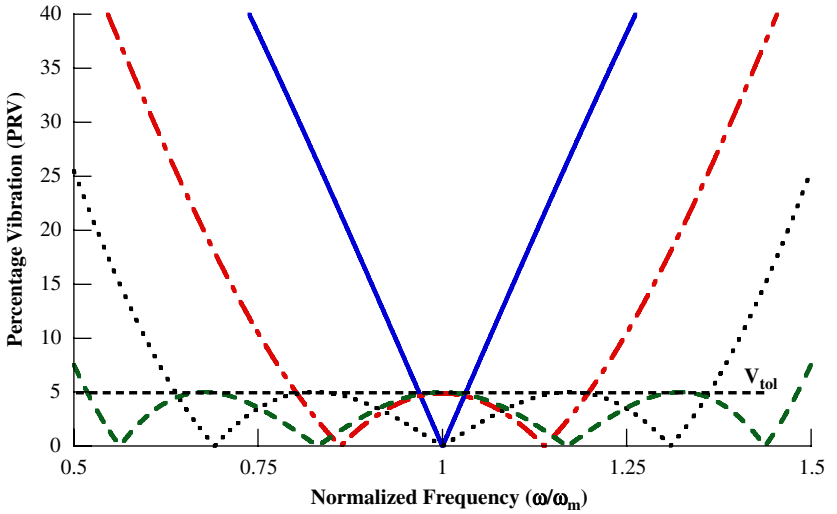

Fig. 4. Sensitivity curves for extra insensitive method shapers, – zero vibration, – · – extra insensitive, … two-hump extra insensitive, – – three-hump extra insensitive.

where

$$A_1 = 0.24968 + 0.24962V_{\text{tol}} + 0.80008\zeta + 1.23328V_{\text{tol}}\zeta + 0.49599\zeta^2 + 3.17316V_{\text{tol}}\zeta^2, \tag{14}$$

$$A_3 = 0.25149 + 0.21474V_{\text{tol}} - 0.83249\zeta + 1.41498V_{\text{tol}}\zeta + 0.85181\zeta^2 - 4.90094V_{\text{tol}}\zeta^2, \tag{15}$$

and

$$t_2 = \frac{1}{\dfrac{2\pi}{\omega\sqrt{1-\zeta^2}}}\begin{pmatrix} 0.49990 + 0.46159V_{\text{tol}}\zeta + 4.26169V_{\text{tol}}\zeta^2 + 1.75601V_{\text{tol}}\zeta^3 + \cdots \\ +8.57843V_{\text{tol}}^2\zeta - 108.644V_{\text{tol}}^2\zeta^2 + 336.989V_{\text{tol}}^2\zeta^3 \end{pmatrix}. \tag{16}$$

Note that the EI is the same duration as the ZVD shaper, but has much more insensitivity, as demonstrated in Fig. 2.

Shapers that extend this idea have a progressively larger number of humps and are called multi-hump EI shapers [17]. The sensitivity curves for two-hump EI and three-hump EI shapers are shown in Fig. 4. Note that the three-hump EI suppresses vibration over the entire range shown. As with the derivative-method shapers, the price for increased robustness is a corresponding increase in shaper duration. Note, however, that the penalty is not uniform across all shapers. The two-hump EI has the same duration as the ZVDD, and the three-hump EI and ZVDDD have the same durations. However, the EI shapers have much more robustness, as can be seen by comparing Figs. 3 and 4. This tradeoff will be further discussed in Section 3. For undamped systems, the two-hump EI is described by [17]

$$\text{two-hump EI} = \begin{bmatrix} A_i \\ t_i \end{bmatrix} = \begin{bmatrix} A_{12H} & \frac{1}{2} - A_1 & A_2 & A_1 \\ 0 & 0.5\tau & \tau & 1.5\tau \end{bmatrix}, \tag{17}$$

where

$$A_1 \equiv A_{12H} = \frac{3X^2 + 2X + 3V_{\text{tol}}^2}{16X}, \tag{18}$$

and

$$X = \sqrt[3]{V_{\text{tol}}^2\left(\sqrt{1 - V_{\text{tol}}^2} + 1\right)}. \tag{19}$$

Table 1
Multi-hump EI shapers for $V_{tol} = 5$ percent

$t_i = (M_0 + M_1\zeta + M_2\zeta^2 + M_3\zeta^3)\tau,\ \tau = \dfrac{2\pi}{\omega}$
$A_i = M_0 + M_1\zeta + M_2\zeta^2 + M_3\zeta^3$

Shaper		M_0	M_1	M_2	M_3
Two-hump EI	t_2	0.49890	0.16270	−0.54262	6.16180
	t_3	0.99748	0.18382	−1.58270	8.17120
	t_4	1.49920	−0.09297	−0.28338	1.85710
	A_1	0.16054	0.76699	2.26560	−1.22750
	A_2	0.33911	0.45081	−2.58080	1.73650
	A_3	0.34089	−0.61533	−0.68765	0.42261
	A_4	0.15997	−0.60246	1.00280	−0.93145
Three-hump EI	t_2	0.49974	0.23834	0.44559	12.4720
	t_3	0.99849	0.29808	−2.36460	23.3990
	t_4	1.49870	0.10306	−2.01390	17.0320
	t_5	1.99960	−0.28231	0.61536	5.40450
	A_1	0.11275	0.76632	3.29160	−1.44380
	A_2	0.23698	0.61164	−2.57850	4.85220
	A_3	0.30008	−0.19062	−2.14560	0.13744
	A_4	0.23775	−0.73297	0.46885	−2.08650
	A_5	0.11244	−0.45439	0.96382	−1.46000

The undamped, three-hump EI shaper is described by [17]

$$\text{three-hump EI} = \begin{bmatrix} A_i \\ t_i \end{bmatrix} = \begin{bmatrix} A_{13H} & \dfrac{(1-V_{tol})}{4} & 1-2(A_1+A_2) & A_2 & A_1 \\ 0 & 0.5\tau & \tau & 1.5\tau & 2\tau \end{bmatrix}, \tag{20}$$

where

$$A_1 \equiv A_{13H} = \frac{1+3V_{tol}+2\sqrt{2V_{tol}(V_{tol}+1)}}{16}. \tag{21}$$

The amplitudes and time locations for the damped two-hump EI ($V_{tol} = 5$ percent) shaper and the three-hump EI ($V_{tol} = 5$ percent) shaper are given in Table 1 as a function of system damping. The curve fits for the two-hump EI shaper have maximum errors in the impulse times and amplitudes of less than 0.5 percent over the range $0 \leqslant \zeta \leqslant 0.3$. The curve fits for the three-hump EI shaper are accurate to within 0.4 percent over the range $0 \leqslant \zeta \leqslant 0.2$.

2.3. Specified insensitivity methods

It is desirable to tailor the robustness of a shaper to the specific system for which it is being designed. The specified insensitivity (SI) shaper does this by generating constraint equations to match the desired level of robustness [10]. An SI shaper can be generated for any desired level of insensitivity in one of two ways. The first is an approximation method in which the vibration is limited to below some tolerable level at several points over the range of parameters desired. Shaper impulse amplitudes and times are then generated using optimization routines. In practice, a small number of points can be used to effectively suppress vibration over a wide range of parameters. The second procedure is more complicated and more difficult to implement but it obtains exact solutions [10].

SI shapers provide the greatest level of robustness for any given shaper duration, a point that will be further discussed in Section 3. Another advantage of SI shapers is that they can be designed to have non-symmetric sensitivity curves, such that the shaper is more robust to increases in frequency than decreases, or vice versa.

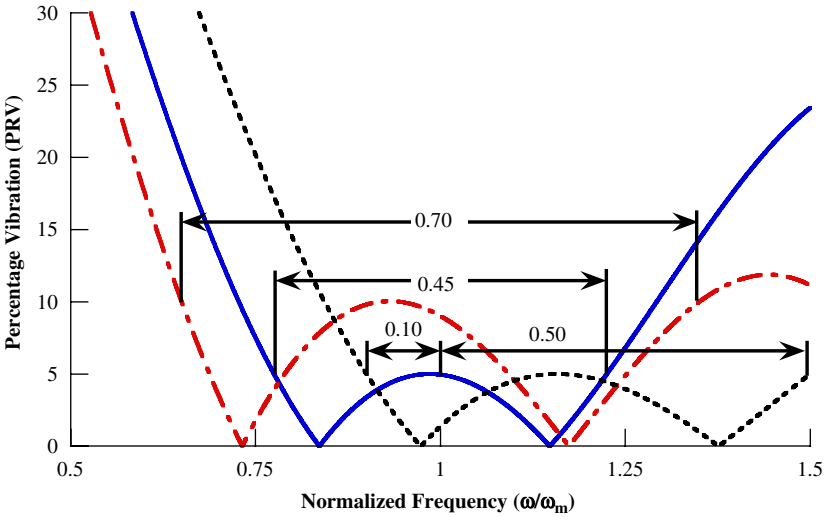

Fig. 5. Sensitivity curves for specified insensitivity shapers, – specified insensitivity $I(5\text{ percent}) = 0.45$, – · – specified insensitivity $I(10\text{ percent}) = 0.70$, … specified insensitivity $I_{\text{low}}(5\text{ percent}) = 0.10$, $I_{\text{high}}(5\text{ percent}) = 0.50$.

SI shapers can also be designed for any level of tolerable vibration. The sensitivity curves for three SI shapers are shown in Fig. 5, including one designed to have an insensitivity of 0.7 for $V_{\text{tol}} = 10$ percent ($I(10\text{ percent}) = 0.7$) and one with a non-symmetric insensitivity region (SI ($I_{\text{low}} = 0.1, I_{\text{high}} = 0.5$)). The non-symmetric SI shaper was designed to be five times more robust to increases in natural frequency than decreases. Its total insensitivity is 0.6, but 0.5 of this lies above the design frequency.

One disadvantage of the SI shaper is that an optimization is required to solve for the impulse amplitudes and time locations. All other shapers discussed in this paper exist in closed form. This disadvantage, however, is a minor inconvenience. Any number of commonly available software packages can perform the relatively easy optimization.

2.4. MIS methods

A modified input-shaping (MIS) technique has been proposed that relaxes the constraint requiring the use of the minimum number of impulses [18]. This technique forms MISZV shapers that have zero vibration at the modeled frequency, but have a larger number of impulses and a longer shaper duration than the ZV shaper (which results from limiting the MISZV shaper to two impulses). An N-impulse MISZV shaper is described by

$$\text{N-impulse MISZV} = \begin{bmatrix} A_i \\ t_i \end{bmatrix} = \begin{bmatrix} \frac{1}{1+M} & \frac{K_m}{1+M} & \cdots & \frac{K_m^{i-1}}{1+M} & \frac{K_m^{N-1}}{1+M} \\ 0 & \frac{\tau_d}{N} & \cdots & \frac{(i-1)\tau_d}{N} & \frac{(N-1)\tau_d}{N} \end{bmatrix}, \tag{22}$$

where $K_m = \mathrm{e}^{-2\zeta\pi/N\sqrt{1-\zeta^2}}$ (note this is slightly different than the previous K), $M = K_m + \cdots + K_m^{i-1} + K_m^{N-1}$, and $\tau_d = 2\pi/\omega\sqrt{1-\zeta^2}$. The sensitivity plots for two- through five-impulse MISZV shapers are shown in Fig. 6. One can see that the additional impulses only provide a minimal increase in shaper insensitivity.

Zero-derivative MIS (MISZVD) shapers are formed by convolving two MISZV shapers designed for the same frequency. The resulting MISZVD shaper is indicated by the number of impulses of each of the MISZV shapers used to create it. An $N \times M$-impulse MISZVD is formed by convolving an MISZV shaper containing N impulses with an MISZV shaper with M impulses. Convolving MISZV shapers of higher number of impulses results in more robust MISZVD shapers, at the cost of increased shaper duration. It should be noted that a 2×2-impulse MISZVD shaper is the traditional ZVD shaper. The sensitivity plots for various MISZVD shapers are shown in Fig. 7.

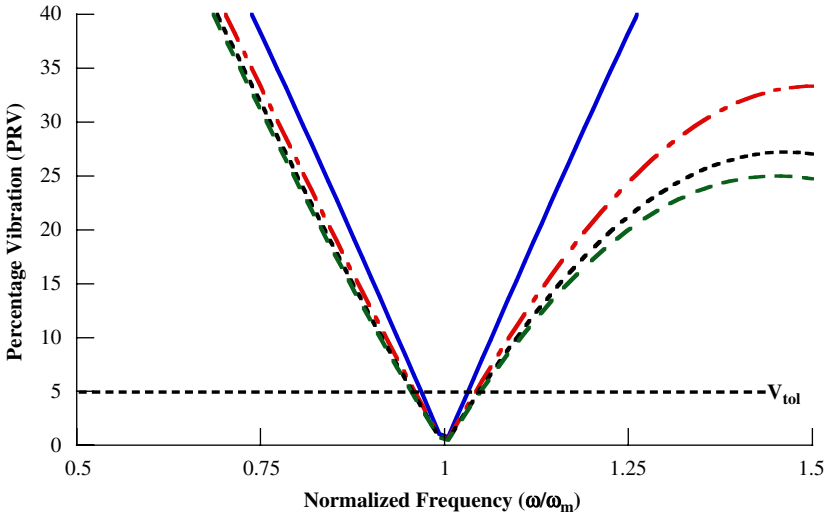

Fig. 6. Sensitivity curves for modified input-shaping-zero vibration shapers, – zero vibration, – · – three-impulse modified input-shaping-zero vibration, ... four-impulse modified input-shaping-zero vibration, – – five-impulse modified input-shaping-zero vibration.

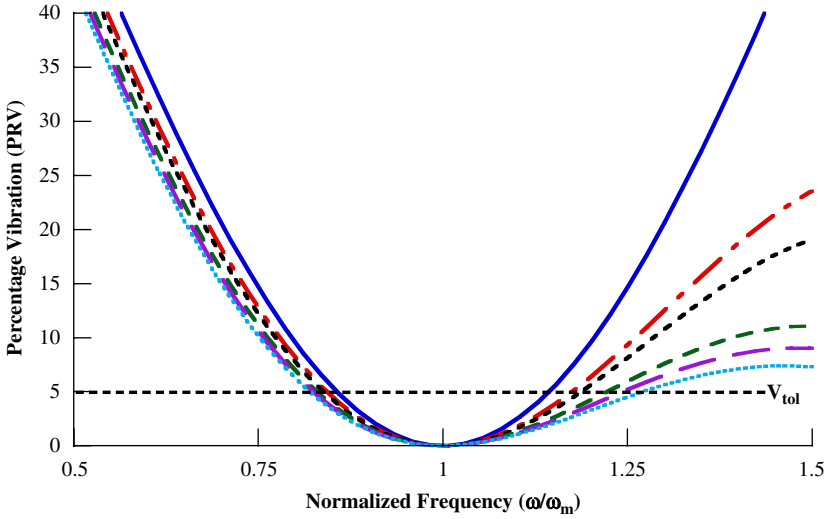

Fig. 7. Sensitivity curves for modified input-shaping-zero vibration and derivative shapers, – zero vibration and derivative, – · – 2×3 modified input-shaping-zero vibration and derivative, - - - 2×4 modified input-shaping-zero vibration and derivative, – – 3×3 modified input-shaping-zero vibration and derivative, — — 3×4 modified input-shaping-zero vibration and derivative, ... 4×4 modified input-shaping-zero vibration and derivative.

3. Shaper insensitivity versus shaper duration

For each method of generating robust input shapers, the shaper duration has increased with insensitivity. The insensitivity for a given shaper duration, however, differs between design methods, indicating the need to thoroughly understand the insensitivity/duration tradeoff between the various shaping methods. To ensure that this analysis is system independent, the shaper duration is normalized by the damped natural period of the system. A shaper with a duration equal to the modeled damped natural period, like the ZVD and EI shapers, has a normalized duration of one.

Fig. 8 shows the 5 percent insensitivity, $I(5 \text{ percent})$, defined in Section 1.2, of various shapers as a function of normalized shaper duration. The SI shaper is plotted as a line, because it can be designed to have any

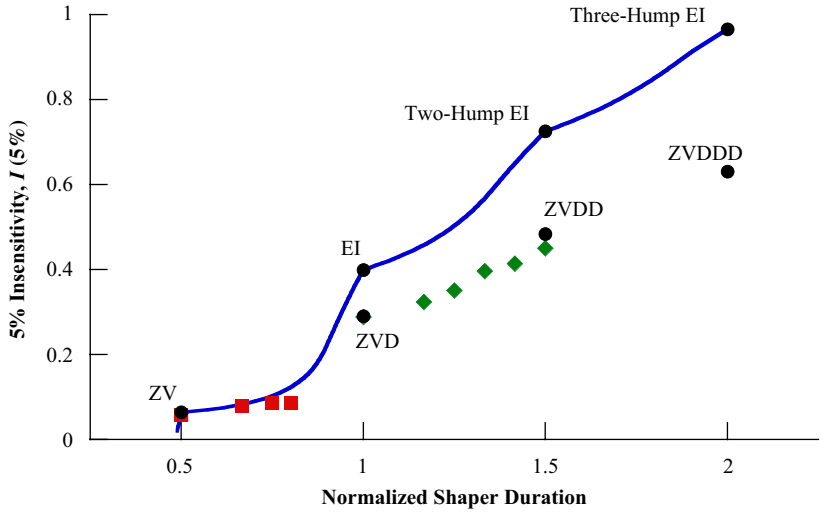

Fig. 8. Insensitivity as a function of normalized shaper duration, – specified insensitivity, ■ modified input shaping-zero vibration, ◆ modified input shaping-zero vibration and derivative.

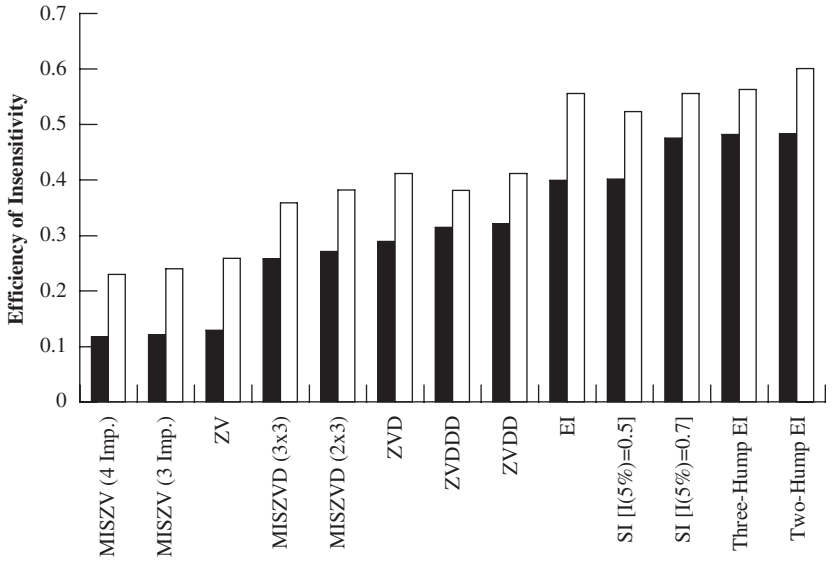

Fig. 9. Efficiency of insensitivity, ■ $I(5\text{ percent})/T_s$, □ $I(10\text{ percent})/T_s$.

desired level of insensitivity. To generate the line, SI shapers were designed for $I(5\text{ percent})$ over the range of parameters shown in the plot, for $I(5\text{ percent}) = 0.02$–$0.970$ at 0.005 increments. The SI shaper has the minimum duration for any given insensitivity. Therefore, SI shapers will provide the fastest rise time. Other shapers discussed in this paper are also shown on the plot. One point of interest is that the EI shapers correspond to nodes on the SI shaper curve. This indicates that they offer the optimal insensitivity for a given shaper duration. It is also of interest to note that both the derivative and MIS methods yield shapers that provide substantially less insensitivity than EI and SI shapers.

In order to further quantify the compromise between insensitivity and shaper duration, the *efficiency of insensitivity* is introduced. The efficiency of insensitivity is the insensitivity of a shaper divided by its normalized duration. Higher numbers indicate that a shaper achieves its robustness more efficiently, in terms of shaper duration. The efficiency of insensitivity for 5 and 10 percent vibration tolerance levels is shown in

Fig. 9. The shapers are sorted from left to right in terms of increasing efficiency of insensitivity for $V_{tol} = 5$ percent.

As seen in Fig. 9, all ZV method shapers, including the MISZV shapers with additional impulses, exhibit a low efficiency of insensitivity for $V_{tol} = 5$ percent. The efficiency values range between 0.1228 for the four-impulse MISZV and 0.1296 for the ZV. Similar trends exist when $V_{tol} = 10$ percent. This indicates that of the shapers with low robustness, the ZV shaper achieves its insensitivity most efficiently.

The evaluation of the efficiency of insensitivity for derivative (ZVD) and MISZVD shapers follows the same trend as the ZV method shapers. For $V_{tol} = 5$ percent, the efficiency of insensitivity of derivative (ZVD) method shapers is greater than that of MISZVD shapers of comparable duration. A similar trend exists when $V_{tol} = 10$ percent.

An obvious result from Fig. 9 is that the SI and EI shapers, which offer optimal insensitivity for a given shaper duration, also provide the highest efficiency of insensitivity, as would be expected. This provides strong evidence that these shapers should be used whenever possible.

4. Robustness to errors in damping

To this point, only robustness to errors in natural frequency has been discussed. Input shaper robustness to errors in damping follows very similar trends. One difference between the frequency sensitivity plots and the damping ratio plots is that the damping ratio is not normalized. This is because when the modeled damping ratio, ζ, is near zero, small changes in the actual damping ratio, ζ_{act}, result in large changes in the normalized damping ratio, ζ/ζ_{act}. Therefore, insignificant changes in system dynamics, say between $\zeta_{act} = 0.001$ and 0.002, show up as large changes in the normalized damping ratio.

The damping sensitivity curves for the ZV and MISZV shapers designed for a damping ratio of 0.1 are shown in Fig. 10. One can see that the ZV and MISZV shapers, which are relatively non-robust to errors in natural frequency, are also relatively non-robust to errors in damping. This trend continues across all shaping methods; robustness to errors in natural frequency generally translates into robustness to errors in damping. This is seen in the plots of the sensitivity of the derivative-method shapers (including MISZVD) in Fig. 11. Notice that the derivative methods have zero slope at the modeled damping ratio and provide a dramatic reduction in vibration for all values of damping shown.

The damping ratio sensitivity curves for the EI-method shapers are shown in Fig. 12. Above damping ratios of approximately 0.175, the vibration levels are lower for longer shaper durations (and higher hump numbers),

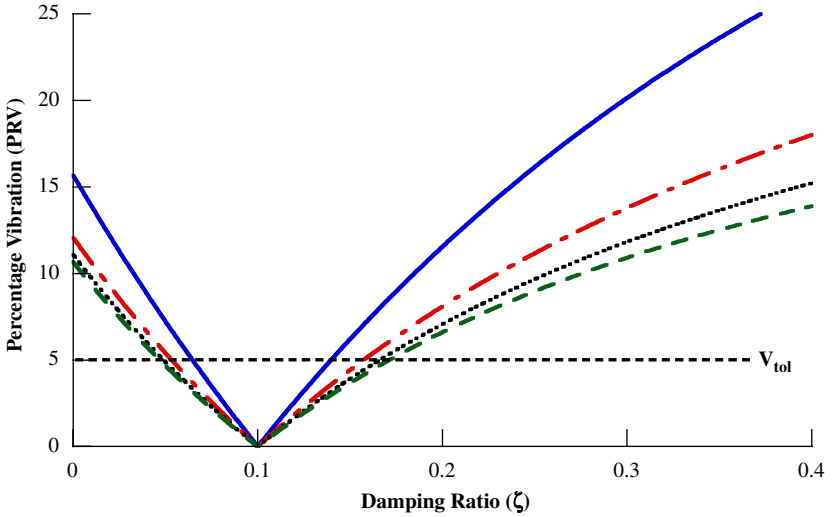

Fig. 10. Damping ratio sensitivity for zero vibration and modified input-shaping-zero vibration shapers ($\zeta_m = 0.1$), – zero vibration, – · – three-impulse modified input-shaping-zero vibration, … four-impulse modified input-shaping-zero vibration, – – five-impulse modified input-shaping-zero vibration.

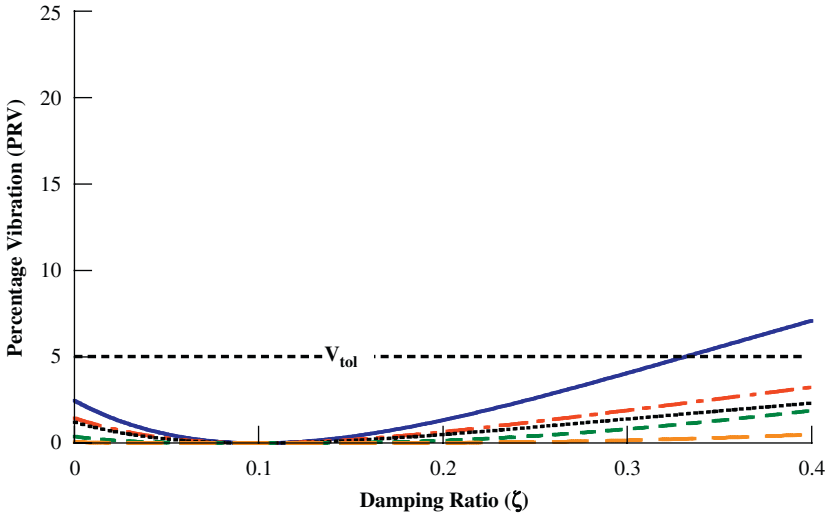

Fig. 11. Damping ratio sensitivity for derivative and modified input-shaping-zero vibration and derivative-method shapers ($\zeta_m = 0.1$), – zero vibration and derivative, – · – 3×3 modified input-shaping-zero vibration and derivative, … 4×4 modified input shaping-zero vibration and derivative, – – zero vibration and double derivative, — — zero vibration and triple derivative.

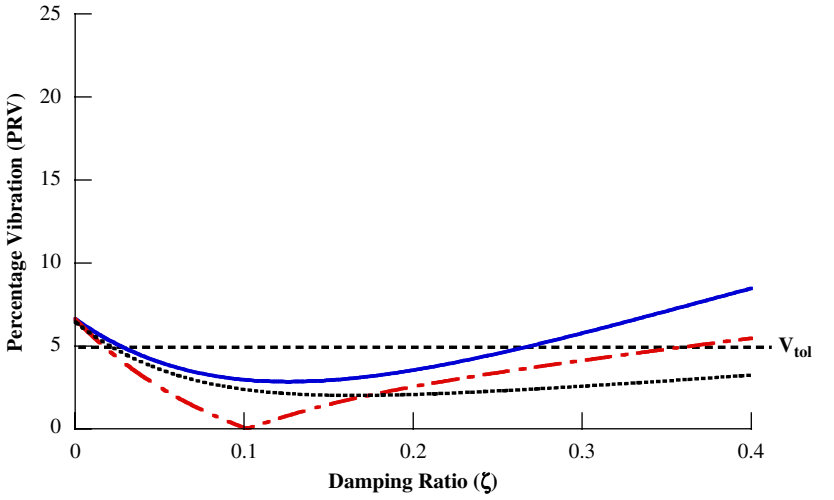

Fig. 12. Damping ratio sensitivity for extra insensitive method shapers ($\zeta_m = 0.1$), – extra insensitive, – · – two-hump extra insensitive, ··· three-hump extra insensitive.

similar to the trends seen in the natural frequency sensitivity plots. However, below 0.175 the level of vibration cannot be predicted solely by shaper duration. Notice that the EI shapers suppress vibration over nearly the entire range of damping ratios shown in the plot. The EI-method shapers in Fig. 12 were designed for a $V_{\text{tol}} = 3$ percent, using Eq. (13) and the formulas from Table 1. This illustrates the flexibility of the EI-method shapers to design for differing tolerable vibration limits. It is also illustrative of the steps that a designer should take when designing EI-method shapers for systems with dramatically varying damping ratios. One can see from Eqs. (13) and (16) that choosing a lower V_{tol} has very little effect on shaper duration; there is little negative consequence to this choice.

The SI shaper, which was discussed with respect to errors in natural frequency in Section 2.3, can also be designed to have an specified insensitivity to damping. Additionally, insensitivity to errors in damping and frequency can be designed into the same SI shaper. This is done in a manner similar to that discussed in

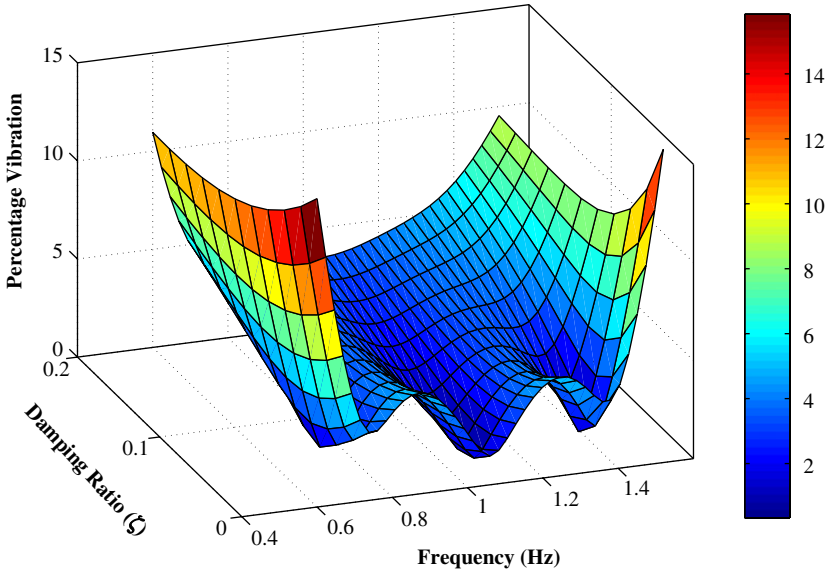

Fig. 13. Three-dimensional sensitivity curve for a specified insensitivity shaper.

Fig. 14. Portable bridge crane.

Section 2.3, by limiting the vibration to below V_{tol} at points within the (ω, ζ) parameter space. Fig. 13 shows a three-dimensional sensitivity curve for an SI shaper that was designed to suppress vibration between 0.7 and 1.3 Hz and also over the range of damping ratios between 0 and 0.2.

5. Experimental comparison of robust shapers

To this point, all results presented have been theoretical. To rigorously test the various shaping methods, representative shapers from each method were experimentally evaluated using the portable bridge crane shown in Fig. 14. The portable bridge crane has a workspace of approximately 1 m × 1 m × 1.6 m. The overhead bridge and trolley are driven using Siemens synchronous AC servo motors attached to timing belts that provide motion in the x and y directions. The motors are controlled using a Siemens PLC using proportional-plus-integral (PI) control with feedback from motor-mounted encoders. The crane is also equipped with a vision system to track payload position.

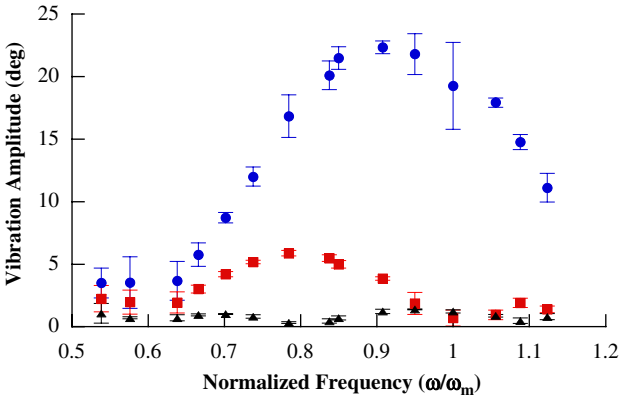

Fig. 15. Vibration amplitudes for unshaped, zero vibration, and specified insensitivity shaped motion, • unshaped, ■ zero vibration, ▲ specified insensitivity.

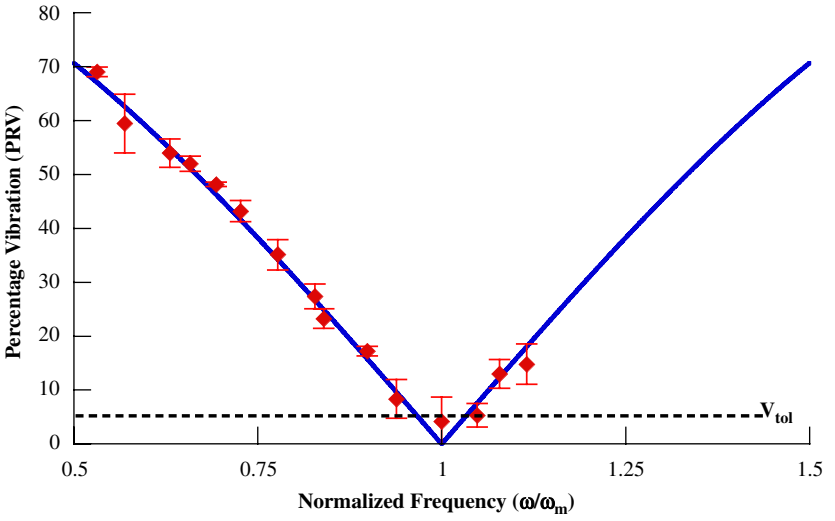

Fig. 16. Experimental sensitivity of zero vibration shaper, – theoretical, ◆ experimental.

Input shapers were designed for a system natural frequency of 0.74 Hz and zero damping, corresponding to a suspension length of approximately 0.46 m (18 in). Seven shapers were tested: ZV, ZVD, EI, two-hump EI, four-impulse MISZV, 2 × 3 MISZVD, and an SI shaper designed with $I(5\text{ percent}) = 0.5$.

The vibration amplitudes for unshaped point-to-point move of approximately 0.6 m is shown in Fig. 15. The vibration amplitude is plotted on the vertical axis. Along the horizontal axis, the different natural frequencies resulting from varying the payload suspension cable length are normalized by the shaper design frequency. The points in this figure and the remaining figures in this paper are averages of three trials. The error bars represent one standard deviation above and below the average value. Average vibration amplitude for unshaped moves varied between 4° and 23° as the suspension length was changed. Also shown in Fig. 15 is the vibration amplitudes for ZV- and SI-shaped motions over the same move distance as the unshaped case. One can see that both the ZV- and SI-shaped vibration amplitudes remained much smaller than the unshaped motion over the entire range of suspension lengths. Even the relatively non-robust ZV shaper greatly reduced the level of vibration over the entire range of cable lengths tested.

The theoretical and experimental sensitivity curves for the ZV shaper are shown in Fig. 16. One can see that the experimental results closely match those predicted by theory. There are more data points at lower

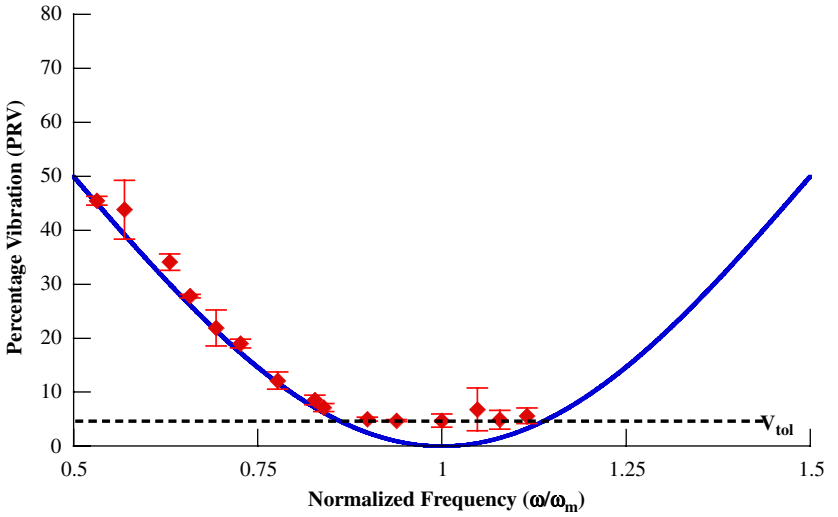

Fig. 17. Experimental sensitivity of zero vibration and derivative shaper, – theoretical, ◆ experimental.

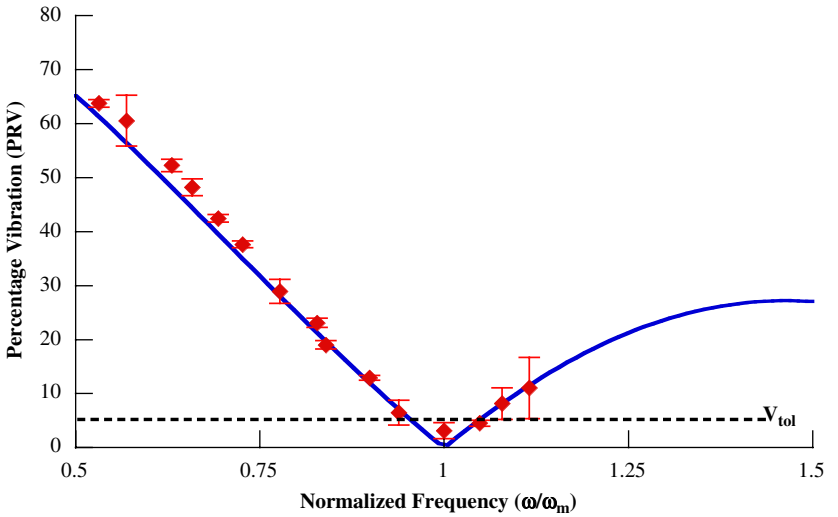

Fig. 18. Experimental sensitivity of a four-impulse modified input-shaping-zero vibration shaper, – theoretical, ◆ experimental.

normalized frequencies due to the nature of the experimental setup. To achieve higher natural frequencies the suspension cable must be shortened. Shortening this cable toward its minimum length makes it impossible for the vision system to track the system response because the payload swings out of the camera's field of view. No such problem exists for longer suspension cable lengths, which result in frequencies lower than the shaper design frequency.

The experimental sensitivity curve for the ZVD shaper is shown in Fig. 17. It too closely matches the predicted behavior; however, even at the modeled frequency the percentage residual vibration is very near the 5 percent V_{tol} level. This corresponds to the noise level in payload swing and camera measurements. This result is not very troubling because even 10 percent vibration is very small—after all, that is a 90 percent reduction in vibration from the unshaped case. It does, however, provide further support for the use of tolerable vibration methods, because zero vibration cannot be achieved in practice.

Figs. 18 and 19 show the experimental and theoretical sensitivity curves for the four-impulse MISZV and 2×3-impulse MISZVD shapers. For each, the experimental results closely follow the theoretical. As with the

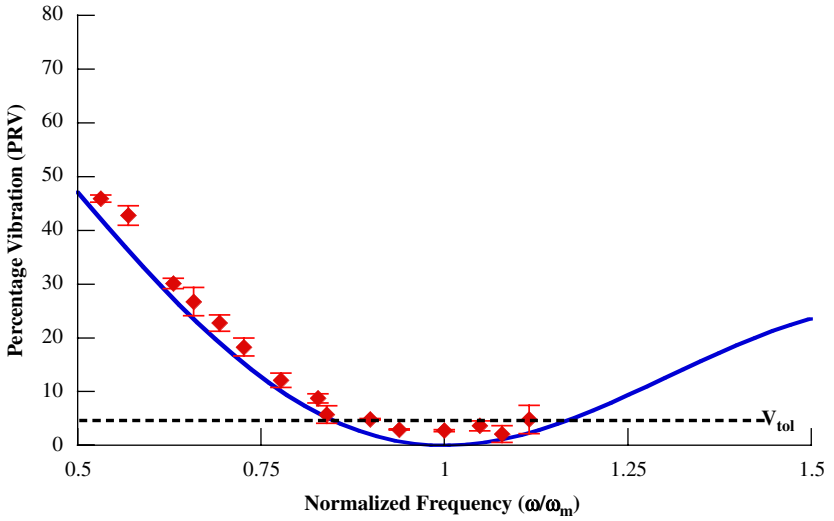

Fig. 19. Experimental sensitivity of 2 × 3 modified input-shaping-zero vibration and derivative shaper, – theoretical, ◆ experimental.

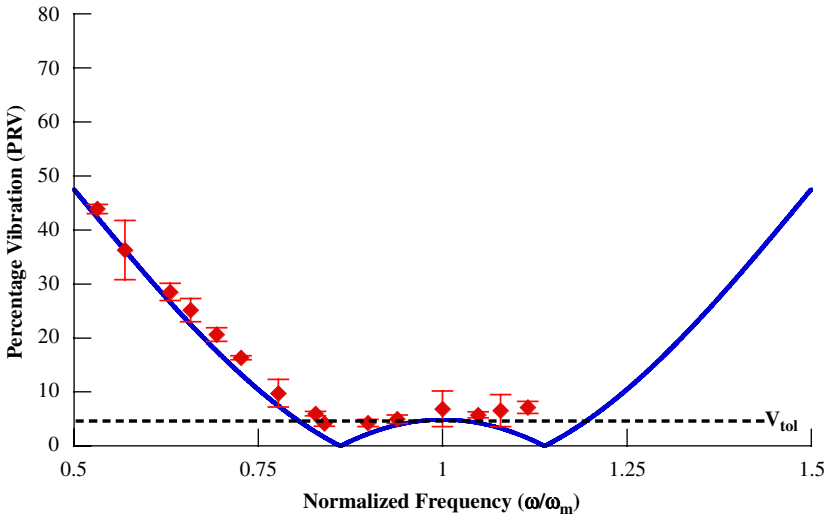

Fig. 20. Experimental sensitivity of extra insensitive shaper, – theoretical, ◆ experimental.

ZV and ZVD shapers, the vibration never reaches the theoretical minimum of zero. The 2 × 3-impulse MISZVD, however, exhibits good robustness to modeling errors in natural frequency, remaining below the V_{tol} over a large range of suspension lengths.

The results for the EI and two-hump EI shapers are shown in Figs. 20 and 21, respectively. Again, the experimental behavior closely follows the theoretical predictions. The two-hump EI shaper provides great reduction in vibration levels over the entire range of suspension lengths, remaining below or only slightly larger than V_{tol} over nearly the entire range. Note that the two-hump EI provides robustness over such a wide range that the experimental setup cannot be changed enough to cause any significant vibration.

The experimental sensitivity curve for an SI shaper designed for an $I(5 \text{ percent}) = 0.5$ is shown in Fig. 22. Like the two-hump EI shaper, vibration is substantially reduced over nearly the entire range of cable lengths. For both the two-hump EI and SI shapers, only extreme changes in cable lengths resulted in vibration levels much greater than V_{tol}. For all shapers, it is important to note that deviation from theory usually occurs such that the actual percentage vibration is slightly larger than predicted by theory. This further reinforces the

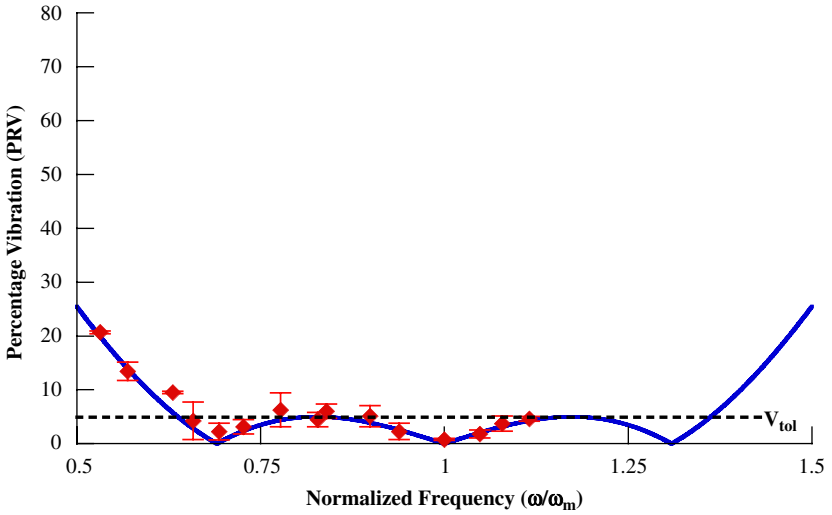

Fig. 21. Experimental sensitivity of two-hump extra insensitive shaper, – theoretical, ◆ experimental.

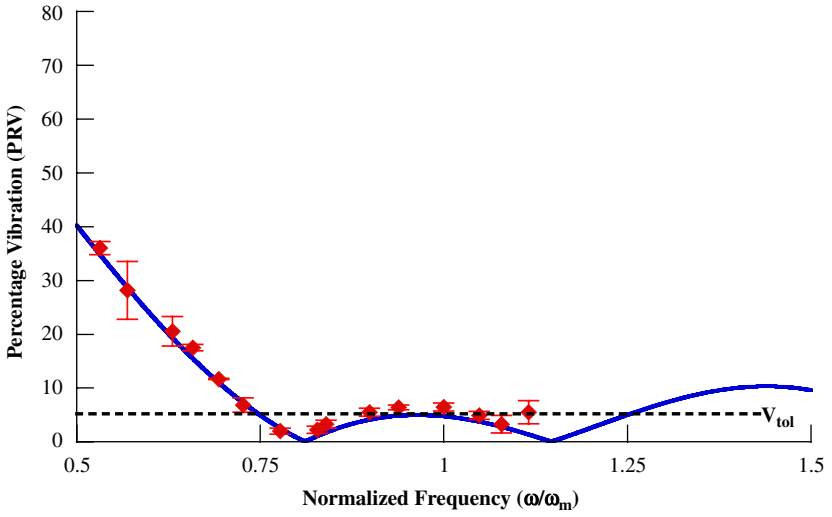

Fig. 22. Experimental sensitivity of specified insensitivity [I(5 percent) = 0.5] shaper, – theoretical, ◆ experimental.

necessity of including robustness in the shaper design process and suggests that, where applicable, V_{tol} should be set slightly low during the shaper design process to ensure that actual system performance meets the desired vibration tolerances.

A bar graph containing the theoretical and experimental efficiency of insensitivity is shown in Fig. 23. To calculate the experimental efficiency of insensitivity, points within the suppression range of the shaper but slightly over the tolerable amount of vibration were still considered to be suppressed. For all cases, twice the width between the design frequency and the lowest frequency that was suppressed by the shaper was used as a measure of the insensitivity. This practice is consistent with the common sense application of the insensitivity criterion and with the accepted measurement of insensitivity for experimental results. One can see that the experimentally measured efficiency of insensitivities closely match those predicted by the theory, but generally have slightly lower values. The close agreement is expected, considering how closely the experimental sensitivity curves in Figs. 16–22 matched the theoretical. It is also to be expected that the experimental values

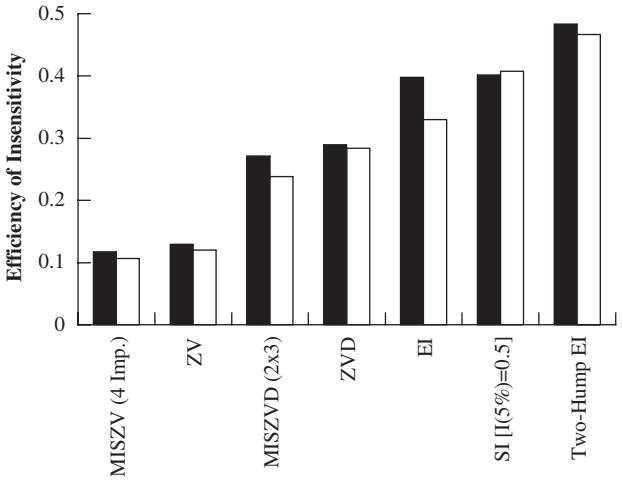

Fig. 23. Theoretical and experimental efficiencies of insensitivity for $V_{\text{tol}} = 5$ percent, ■ theoretical, □ experimental.

are slightly lower than the theoretical values. This is a function of the payload oscillation generally being slightly larger than predicted by theory, as seen in Figs. 16–22.

6. Conclusions

Many robust shaping methods have been proposed. Within each shaping method, increased robustness comes at the expense of increased shaper duration and, as a result, slower system rise time. However, different shaper design methods provide robustness with differing efficiency. This paper presented an analysis of input-shaping methods based upon a new performance measure for input shapers, the efficiency of insensitivity. Using this measure, in conjunction with other shaper performance measures, it was shown that EI and SI shapers most efficiently provide robustness to modeling errors and parameter uncertainty. Hundreds of experimental trials on a portable bridge crane verified the theoretical predictions.

Acknowledgments

The authors would like to thank Siemens Energy and Automation and the Georgia Tech PURA for their support of this work.

References

[1] J. Calvert, D. Gimpel, Method and apparatus for control of system output in response to system input, Patent number: 2,801,351, 1957.
[2] O.J.M. Smith, Posicast control of damped oscillatory systems, *Proceedings of the Institute of Radio Engineers* 45 (9) (1957) 1249–1255.
[3] O. Smith, *Feedback Control Systems*, McGraw-Hill, New York, 1958.
[4] G.H. Tallman, O.J.M. Smith, Analog study of dead-beat posicast control, *Institute of Radio Engineers Transactions on Automatic Control* 4 (1) (1958) 14–21.
[5] K. Kozak, W. Singhose, I. Ebert-Uphoff, Performance measures for input shaping and command generation, *Journal of Dynamic Systems, Measurement, and Control* 128 (3) (2006) 731–736.
[6] N.C. Singer, W.P. Seering, Preshaping command inputs to reduce system vibration, *Journal of Dynamic Systems, Measurement, and Control* 112 (1990) 76–82.
[7] B. Murphy, I. Watanabe, Digital shaping filters for reducing machine vibration, *IEEE Transactions on Robotics and Automation* 8 (2) (1992) 285–289.
[8] W. Singhose, W. Seering, N. Singer, Residual vibration reduction using vector diagrams to generate shaped inputs, *Journal of Mechanical Design* 116 (2) (1994) 654–659.
[9] T. Singh, S.R. Vadali, Robust time-delay control of multimode systems, *International Journal of Control* 62 (6) (1995) 1319–1339.

[10] W.E. Singhose, W.P. Seering, N.C. Singer, Input shaping for vibration reduction with specified insensitivity to modeling errors, *Proceedings of Japan– USA Symposium on Flexible Automation*, Boston, MA, June 1996.
[11] U.-H. Park, J.-W. Lee, B.-D. Lim, Y.-G. Sung, Design and sensitivity analysis of an input shaping filter in the z-plane, *Journal of Sound and Vibration* 243 (1) (2001) 157–171.
[12] W. Singhose, W. Seering, N. Singer, Shaping inputs to reduce vibration: a vector diagram approach, *Proceedings of IEEE International Conference on Robotics and Automation*, Vol. 2, Cincinnati, OH, May 1990, pp. 922–927.
[13] J. Lawrence, W. Singhose, Decreasing effects of coulomb friction in precision positioning using input shaping: experimental verifications, *Proceedings of Japan– USA Symposium on Flexible Automation*, Hiroshima, Japan, July 2002.
[14] J. Smith, K. Kozak, W. Singhose, Input shaping for a simple non-linear system, *Proceedings of 2002 American Control Conference*, Anchorage, AK, May 2002.
[15] D.F. Blackburn, W. Singhose, J.P. Kitchen, V.P. Petrangenaru, J. Lawrence, T. Kamoi, A. Taura, Advanced input shaping algorithm for nonlinear tower crane dynamics, *8th International Conference on Motion and Vibration Control*, Daejeon, Korea, 2006.
[16] P.H. Meckl, P.B. Arestides, M.C. Woods, Optimized s-curve motion profiles for minimum residual vibration, *Proceedings of American Control Conference*, Philadelphia, PA, 1998.
[17] W.E. Singhose, L.J. Porter, T.D. Tuttle, N.C. Singer, Vibration reduction using multi-hump input shapers, *ASME Journal of Dynamic Systems Measurement and Control* 119 (2) (1997) 320–326.
[18] J. Shan, H.-T. Liu, D. Sun, Modified input shaping for a rotating single-link flexible manipulator, *Journal of Sound and Vibration* 285 (1–2) (2005) 187–207.